

# Experimental investigation of local heat transfer in a square duct with various-shaped ribs

Lei Wang · Bengt Sundén

Received: 9 March 2005 / Accepted: 16 June 2006 / Published online: 6 October 2006  
© Springer-Verlag 2006

**Abstract** In the present study, experimental studies are carried out to investigate the heat transfer and friction characteristics in a square duct roughened by various-shaped ribs on one wall. The ribs are oriented transversely to the main stream in a periodic arrangement. Liquid crystal thermography is employed to measure the local and average heat transfer coefficient on the ribbed surface. The rib height-to-duct hydraulic diameter ratio is fixed at 0.1; the rib pitch-to-height ratio varies from 8 to 15 and the test Reynolds number spans from 8,000 to 20,000. The results show that the trapezoidal-shaped ribs with decreasing height in the flow direction (case C) provide the highest heat transfer enhancement factor and are likely to be used to suppress the local hot spot which usually occurs in the region just behind the ribs.

## 1 Introduction

Periodic ribs are frequently employed to enhance the heat transfer process in various cooling passages, e.g., of turbine blades, guide vanes, and combustor walls. However, the increase in heat transfer is usually accompanied with a rise in pressure drop. In the design and manufacturing of gas turbines, it is desirable to predict the heat transfer coefficient and friction factor by means of theoretical approaches. When the rib height to hydraulic diameter ratio is small, the

repeated-rib surface can be considered as a rough surface geometry. Based on the law of the wall, a one-dimensional analysis was developed to correlate the friction factor and heat transfer coefficient by Nikuradse [1] and Dipprey and Sabersky [2], respectively. The effect of the geometrically non-similar roughness parameter, the rib pitch to height ratio, was first studied by Webb et al. [3]. The successful prediction model for the average heat transfer coefficient and friction factor in channels with two opposite rib-roughened walls was formulated by Han [4]. More recently, Chandra et al. [5] extended the past predictions to the cases of varying number of ribbed walls in a square channel. However, Rau et al. [6] pointed out that the valid range for the application of Han's formula was actually limited to  $e/D_h < 0.0625$ .

With larger rib height and aspect ratio close to unity, a more three-dimensional flow including flow separation, reattachment as well as redevelopment, makes it hard to predict the heat transfer coefficient only by virtue of the one-dimensional similarity analysis. For example, Webb et al. [3] showed that the heat transfer coefficient attains its maximum value in the vicinity of the reattachment point. Liou and Hwang [7], however, observed the deterioration of heat transfer in the region just behind the ribs due to the formation of hot spot. Therefore, more detailed information on flow structure and local heat transfer data in rib-roughened channels is required for designers and researchers to optimize the cooling technique.

Many experimental investigations have been carried out to determine configurations that produce optimum results in terms of both heat transfer and friction factor. One of the most important attempts is to examine the rib geometry which gives the best heat transfer per-

---

L. Wang · B. Sundén (✉)  
Heat Transfer Division, Lund Institute of Technology,  
Box 118, Lund 221 00, Sweden  
e-mail: Bengt.Sunden@vok.lth.se

formance for a given flow friction. Lockett and Collins [8] investigated the heat transfer distribution and associated hot spots around square- and rounded-rib geometries. Due to the more streamlined shape for the rounded rib, the sharp decrease in heat transfer at the rear of the square rib disappeared and was replaced by a more gradual change. They also found that the heat transfer distribution was more uniform downstream the reattachment point for the rounded rib geometry. Han et al. [9] applied modeling clay to fill the corners of the rectangular ribs to create two distinct geometries. It was found that the clay has much more modest effect on the heat transfer coefficients than on the friction factor, and the influence of the rib shape on the Stanton number disappears at higher Reynolds number where the flow is in the completely rough regime. Liou and Hwang [10] examined the fully developed flow in channels roughened with three rib shapes, namely square, semicircular and triangular cross section. The results showed that the lowest friction factor was obtained for the semicircular-ribbed case because this was the most streamlined rib shape. Additionally, the triangular-ribbed, semicircular-ribbed and square-ribbed geometries have comparable thermal performance, but the square-ribbed geometry is the most likely one to yield hot spots around the rear corner behind the rib. Arman and Rabas [11] used a numerical code to determine the thermal-hydraulic performance of enhanced tubes with transverse, periodic sine-, semicircular-, arc-, and trapezoid-shaped disruptions. As expected, a tradeoff between heat transfer and pressure drop was found when the disruption shape became more contoured; that is, both the heat transfer and the pressure drop increase. The pressure drop is more dependent on the disruption shape and it continues to decrease when the disruption become less contoured because of the reduced form drag. Chandra et al. [12] investigated the effect of rib shape on the heat transfer and friction in a square channel. It was shown that the square ribs produce higher heat transfer augmentation for a given friction factor than any other rib profile. In addition, there are extremely small differences in the performance of triangular and slant-edged ribs and the performance of the circular and semicircular ribs. More recently, Ahn [13] studied the fully developed heat transfer and friction characteristics in a rectangular duct roughened by various rib shapes, i.e., square, triangular, circular, and semicircular geometries. Contrary to previous works, he concluded that the triangular-shaped rib has the highest heat transfer performance.

Inspection of the literature reveals that further experimental investigations are required, especially considering the few data of detailed distribution of the

heat transfer coefficient in channels roughened with various-shaped ribs. In general, detailed maps of the local heat transfer coefficient can be obtained by using optical techniques, such as the infra-red thermography (IRT) [14] and the liquid crystal thermography (LCT) [6, 15–16]. Usually, the LCT technique is more economical and affordable than the IRT method. The LCT technique can be classified into two categories: the steady method [6, 15–16] and the transient method [17]. The transient method is based on the fact that when the test surface of uniform initial temperature is suddenly exposed to an isothermal fluid flow, the magnitude of the surface temperature change is governed by one-dimensional transient heat conduction. However, Chang et al. [18] argued that the three-dimensional wall conductivity effect on the temperature measurement over the rib-roughened surface makes the one-dimensional assumption adopted by the transient method invalid. Furthermore, the transient LCT is usually more difficult to conduct than the steady method, which requires a more complicated image processing system. Therefore, the steady-state LCT technique is employed in this study.

This paper basically describes the characteristics of the heat transfer and friction in a square duct roughened by transversely placed, various-shaped ribs on one wall. The shapes of the ribs are square, equilateral-triangular, trapezoidal with decreasing height in the flow direction and trapezoidal with increasing height in the flow direction. The ribs, made of Plexiglas, are considered to be not involved into the heat transfer process due to the low thermal conductivity ( $k = 0.2 \text{ W/mK}$ ). The objectives of this research are to fulfill three aspects; i.e., to assess the occurrence of hot spot on the rib-roughened wall by investigating the effect of rib shape on the distribution of local heat transfer; to provide detailed information of local heat transfer for researchers and engineers to optimize the cooling technique; and to quantify the thermal performance of ducts roughened with various-shaped ribs.

## 2 Experimental apparatus and procedures

### 2.1 Experimental apparatus

#### 2.1.1 Heat transfer test

The experimental apparatus is not shown here for the sake of brevity. Further details can be found in Wang and Sundén [19]. The test section consists of a 750 mm long smooth duct followed by a rib-roughened section

of equal length. Plexiglas plates are applied to provide optical access for liquid crystal measurement. The thickness of the duct wall is 10 mm with internal channel cross-section  $50 \times 50 \text{ mm}^2$ . An Inconel foil with thickness  $12 \text{ }\mu\text{m}$  is applied to produce a uniform heat flux on one wall in the rib-roughened section. The measurements are carried out at the location of approximately  $27 < X/D_h < 29$  from the inlet of duct. Various-shaped ribs are glued on the heated surface; the rib configurations are shown in Fig. 1. The trapezoidal-shaped rib with inclination angle  $38^\circ$  is exhibited in Fig. 2.

The pre-packaged liquid crystal sheet R35C5W (0.15 mm thick) backed with pressure-sensitive adhesive is applied to map the temperature distribution on the ribbed surface. Before the execution of the experiment, the liquid crystal was calibrated to get the relationship between the temperature and the hue value. The detailed description is given in Gao [20]. The hue-temperature calibration data is presented in Fig. 3. It is found that the hue is fairly linear with temperature in the range of 30–150, corresponding to the temperature range of 35–37.5°C. The colour distribution of the liquid crystal is recorded by a CCD camera, from which the image is digitised and transferred for further processing.

### 2.1.2 Pressure test

The test rig consists of the same apparatus as the heat transfer test except there is no heating current present. The distance between the two static pressure taps are eightfold hydraulic diameter along the centreline of the smooth sidewall. The diameter of tapping hole is 1 mm. Short stainless steel tubes are glued in the holes to provide connection with the micromanometer.

### 2.2 Data reduction

The Reynolds number  $Re$ , based on the bulk mean velocity and hydraulic diameter of the square duct, varies from 8,000 to 20,000 in the present test. The Nusselt numbers  $Nu$ , is derived directly from the heat flux and the temperature difference; that is,

$$Nu = \frac{(Q_{el} - Q_{loss})D_h}{(T_w - T_{bulk})k_f A} \quad (1)$$

in which  $Q_{el}$  is the measured input power to the heater,  $Q_{loss}$  is the dissipation rate in terms of radiative heat transfer to the surroundings and the conductive heat transfer through the back of the heated surface. In estimating the radiative heat loss, the surface and air

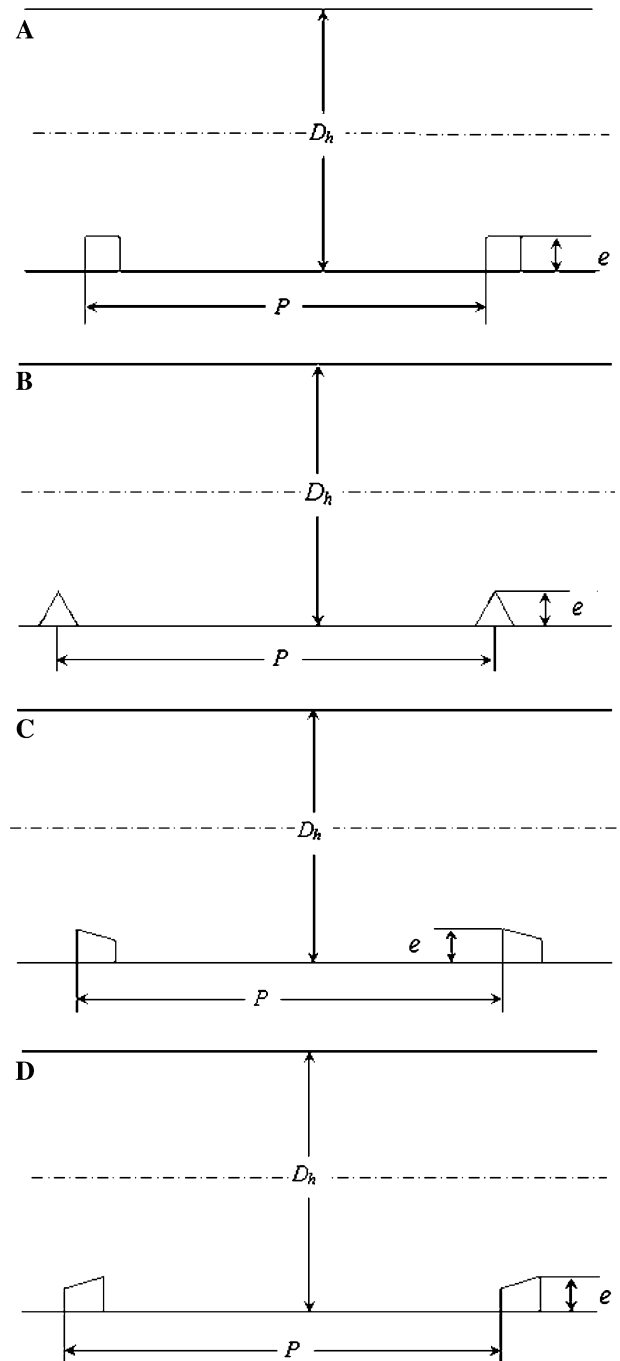


**Fig. 1** Rib configurations; **a** Square ribs **b** Equilateral-triangular ribs **c** Trapezoidal ribs with decreasing height in the flow direction **d** Trapezoidal ribs with increasing height in the flow direction

bulk temperature are considered as constant when considering the fact that the air temperature rise from entrance to exit is less than  $2^\circ\text{C}$ . For polished Inconel, the emissivity is approximately equal to 0.05. The conduction heat leakages are calculated from the temperature difference across the heated wall. Two fine-gauge thermocouples are installed at the back of

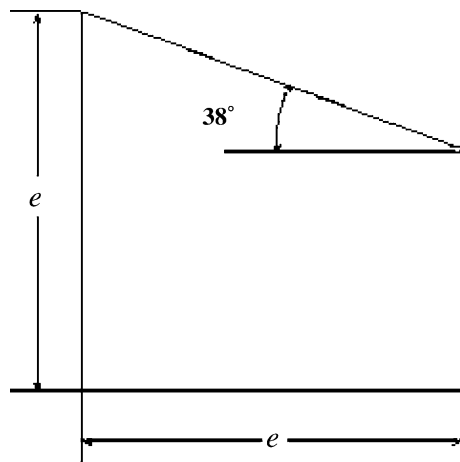


**Fig. 2** Cross-section of the trapezoidal-shaped rib

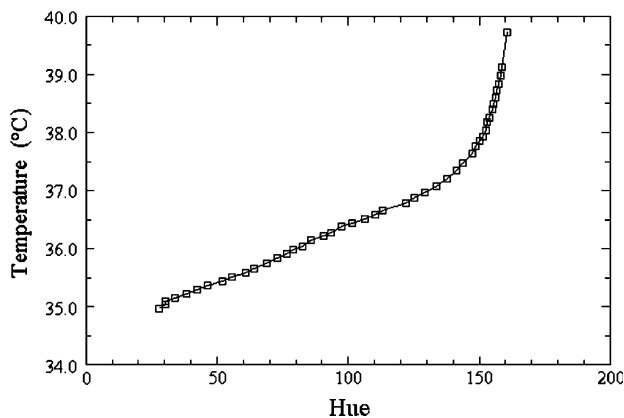


**Fig. 3** Hue-temperature calibration

the heated surface. The sum of the two terms is found to be less than 5% of  $Q_{el}$ . In Eq. 1,  $k_f$  is the air thermal conductivity and  $A$  is the area of the heating surface;  $T_w$  is the surface temperature indicated by the liquid crystal and  $T_{bulk}$  is the local air bulk temperature along the streamwise direction  $X$ ,

$$T_{bulk} = T_{in} + (Q_{el} - Q_{loss}) / (X/L) / \dot{m}c_p \quad (2)$$

In Eq. 2,  $T_{in}$  is the air temperature measured at the entrance of the duct (where the flow is assumed to be isothermal),  $c_p$  is the air specific heat,  $\dot{m}$  is the mass flow rate, and  $L$  is the heated surface length. The thermal properties are evaluated at the average air bulk temperature according to [21]. Typically, the temperature difference between the wall and the bulk air is kept within 13–15°C.

Area-average Nusselt number is calculated according to Eq. 3,

$$Nu_{av} = \sum_{i=1}^N Nu_i \frac{i}{N} \quad (3)$$

in which  $Nu_i$  is the Nusselt number at local pixel and  $N$  is the number of pixels in the considered area. All the Nusselt numbers are normalized with respect to the level obtained in a smooth circular tube (Dittus–Boelter correlation) and presented as the enhancement factor.

$$Nu_0 = 0.023Re^{0.8}Pr^{0.4} \quad (4)$$

The friction factor  $f$ , based on the isothermal conditions, is determined from the slope of the static pressure. All the measured friction factors are normalized with the friction factor of a smooth channel, given by:

$$f_0 = 0.046Re^{-0.2} \quad (6)$$

The following expression,  $(Nu_{av}/Nu_0)/(f/f_0)^{1/3}$  is used to evaluate the thermal performance based on the constant pumping power.

### 2.3 Experimental uncertainty

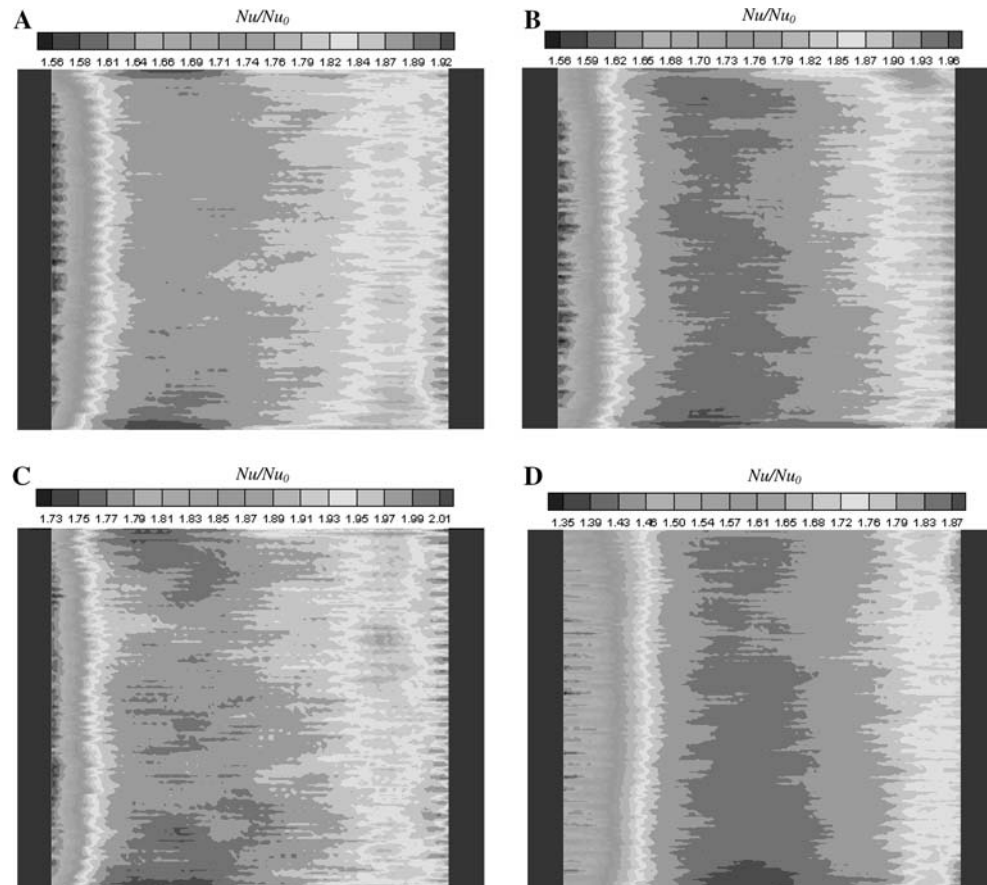
The uncertainty is evaluated according to the method described by Moffat [22]. The uncertainty (based on the normal distribution with 95% confidence) in local  $Nu$  number is estimated to be within  $\pm 6\%$ . This uncertainty value takes into account such independent variables as electric current, resistance of heater, liquid crystal thermographic readings, air bulk temperature, and dissipation rate. The Reynolds number has a calculated uncertainty of  $\pm 3.5\%$ . Finally, the uncertainty in the friction factor  $f$  would lie within  $\pm 4\%$  at the considered Reynolds number.

## 3 Results and discussion

### 3.1 Local heat transfer characteristics

Figure 4 shows the mapping of the local heat transfer enhancement factor for all the rib geometries at the same Reynolds number and pitch ratio ( $Re = 20,000$ ,  $P/e = 12$ ). In each case, the footprints of flow separation, recirculation as well as redevelopment can be observed clearly by the spatial variation of the local heat transfer performance. The minimum Nusselt number, occurring in the region just behind the rib, is due to the low fluid velocity around the corner. A rapid

**Fig. 4** Mapping of the inter-rib local heat transfer distribution for  $P/e = 12$  ( $Re = 20,000$ )



rise of Nusselt number is found in the recirculation region due of the entrainment of cooler fluid towards the wall by the shear layer. Further downstream, the Nusselt number is decaying gradually because the new boundary layer grows in thickness. In order to quantify the local heat transfer features for the investigated rib shapes, the Nusselt number ratios along the centreline are plotted in Fig. 5. It is clearly shown that the trapezoidal ribs of case C have the highest Nusselt number enhancement factors in the whole region. Unexpectedly, the trapezoidal ribs of case D, merely arranged in the opposite direction relative to case C, have the lowest heat transfer rates, especially in the region just downstream the rib. At  $X/e = 1$ , the local heat transfer induced by the trapezoidal ribs of case C is augmented 10% compared to the ordinary-used square ribs (Case A); whereas, in case D, the local heat transfer performance drops 12%. It should be mentioned that the triangular ribs (case B) have similar heat transfer performance as the square ribs. In the zone downstream the reattachment point ( $4 < X/e < 10$ ), the local heat transfer is less dependent on the shape of the rib and the Nusselt number ratios are found to be close to each other. Further inspection of this figure reveals that the location of maximum heat transfer in case C

( $X/e \approx 2$  or 3) is distinct from that of case D ( $X/e \approx 4$  or 5). The shift of the location of maximum heat transfer can be attributed to the different separation angle when the fluid approaches the different windward surface of the upstream rib. A similar result was obtained by Terekhov et al. [23], who carried out experimental studies on the heat transfer characteristics behind backward-facing inclined steps. They found

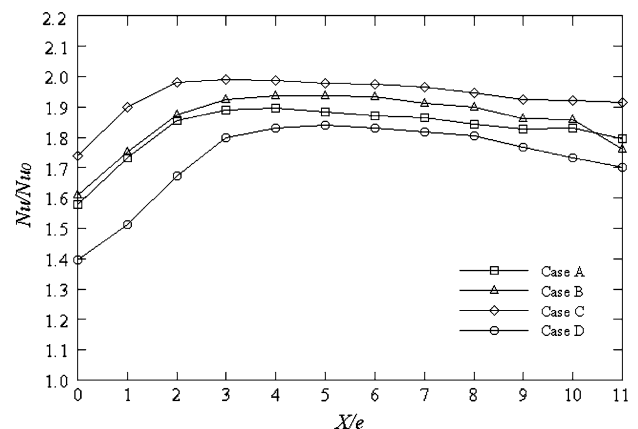


**Fig. 5** Local heat transfer increase along the centerline for  $P/e = 12$  ( $Re = 20,000$ )



under natural-turbulence condition, a decrease in the step-face inclination angle from  $90^\circ$  to  $20^\circ$  leads to the intensification of heat transfer and the shift of the maximum heat-transfer location in the upstream direction.

According to Fig. 5, it is indicated that the trapezoidal-shaped ribs of case C have the highest heat transfer efficiency among the four rib geometries investigated. To conclude on this aspect, the experiment proceeds to study this type to highlight the effect of the rib pitch ratio.

### 3.2 Effect of pitch ratio in case C

Figure 6 displays the mapping of the local heat transfer enhancement factor for various pitch ratios at the same Reynolds number ( $Re = 20,000$ ). Due to the smaller

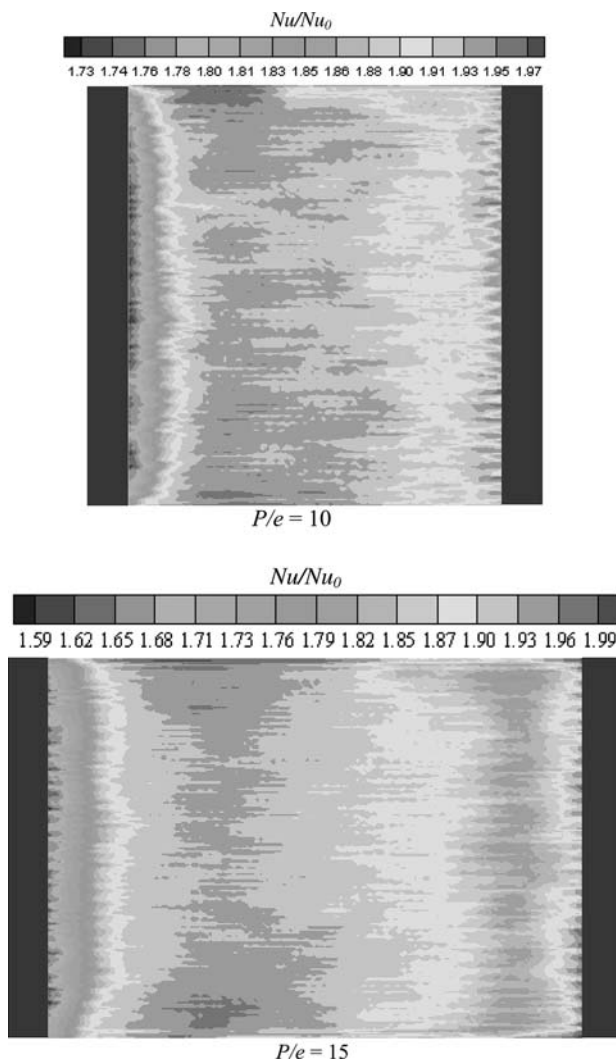


**Fig. 6** Mapping of the inter-rib local heat transfer distribution for  $P/e = 10$  and  $15$  ( $Re = 20,000$ )

rib spacing at  $P/e = 10$ , the boundary layer redevelopment region downstream the reattachment point is obviously decreased. Therefore, the local heat transfer distribution at  $P/e = 10$  is more uniform than that at  $P/e = 15$ . In order to infer the effect of rib spacing on the local heat transfer, the Nusselt number ratios along the centreline are shown in Fig. 7. In the entire region, the  $P/e = 12$  provides the highest heat transfer enhancement factor. In this figure it is also noticed that the local heat transfer in the region just downstream the rib ( $0 < X/e < 2$ ) is nearly the same; that is, the local heat transfer is less dependent on the rib spacing. Further view of this figure shows that the location of maximum heat transfer shifts downstream by increasing the  $P/e$  ratio. For  $P/e = 8, 10$  and  $12$ , the maximum heat transfer location is 2 or 3 rib heights away from the rib edge; whereas, the local maximum heat transfer shifts downstream about 4 rib heights at  $P/e = 15$ . This may be attributed to the decrease of the streamwise pressure gradient as the rib spacing increases.

For higher pitch ratios ( $P/e \geq 12$ ) a second maximum heat transfer rate is observed just in front of the downstream rib, which is in agreement with the results of Rau et al. [6]. This can be explained by the fact that a new boundary layer is built up downstream the reattachment point by the entrainment flow. High momentum fluid is constantly brought into the outer shear layer by the downward motion of the outer flow, thereby continuously increasing the streamwise velocity in this layer [24]. For larger pitch ratios, the longer distance between the reattachment point and the following rib leads to higher momentum. Therefore, in the second separation zone ahead of the rib, the entrainment of relatively cooler and higher momentum fluid from the outer shear layer into this recirculation region causes this second top of the Nusselt number.

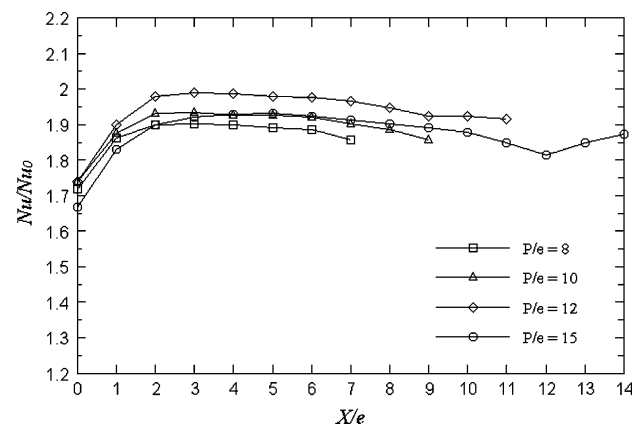


**Fig. 7** Local heat transfer increase along the centerline at  $Re = 20,000$

### 3.3 Comparison of average heat transfer and friction characteristics

The normalized friction factors in a square duct roughened with various-shaped ribs at the same pitch ratio ( $P/e = 12$ ) are plotted in Fig. 8. In the given Reynolds number range, the trapezoidal-shaped ribs of case C have the highest friction loss; whereas, the trapezoidal-shaped ribs of case D have the lowest pressure drop. Furthermore, the triangular-shaped ribs (case B) have slightly higher friction factor than that of square-shaped ribs (case A). Based on the law of the wall similarity, Chandra et al. [5] developed semi-empirical formulas to predict the heat transfer coefficient and friction factor in a square duct roughened by the square-shaped ribs on one wall. The prediction of the friction factor is very close to the result of case C and the maximum deviation from the present data of square ribs is less than 15%.

The normalized average Nusselt numbers in a square duct roughened with various-shaped ribs at  $P/e = 12$  are plotted in Fig. 9. As expected, it is seen that the trapezoidal-shaped ribs of case C have the highest heat transfer enhancement in the considered Reynolds number range. In contrast, the trapezoidal-shaped ribs of case D have the lowest heat transfer performance. Meanwhile, the square-shaped ribs (case A) have nearly the same enhancement factor as the triangular-shaped ribs (Case B). This result is not in line with the conclusions by Ahn [13] who found that the triangular ribs are more efficient in heat transfer than the square ones. The correlation proposed by Chandra et al. [5] fits quite well the present data of square ribs except for the low Reynolds number ( $Re = 8,000$ ).

Figure 10 shows that a square duct roughened with various-shaped ribs has comparable thermal perfor-

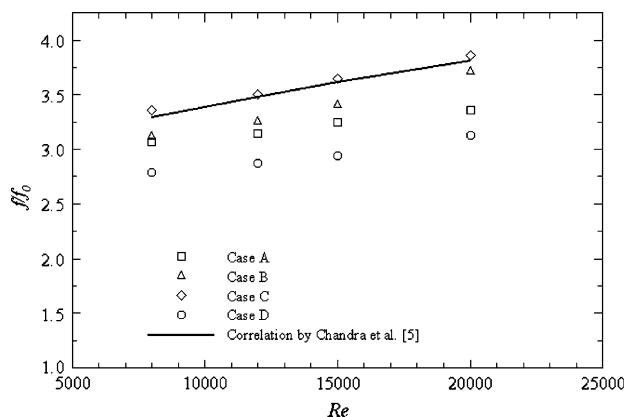


**Fig. 8** Comparison of the friction factor ratios for various-shaped ribs for  $P/e = 12$

mance; that is, the thermal performance is less dependent on the variation of rib shape. The result is in accord with the conclusion of Liou and Hwang [10], even though the rib geometries studied in their experiment are different from the present. In addition, the theoretical prediction of the thermal performance tends to approach the experimental data with increasing Reynolds number and the maximum deviation from the present data at  $Re = 20,000$  is less than 5%.

### 4 Conclusions

The fully developed turbulent heat transfer and friction in a square duct roughened with various-shaped ribs on one wall have been investigated experimentally by using liquid crystal thermography. Based on the experimental results, the conclusions are as follows:

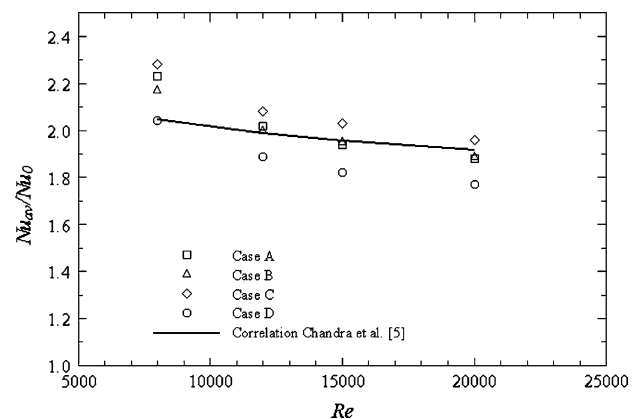


**Fig. 9** Comparison of the average Nusselt number ratios for various-shaped ribs for  $P/e = 12$

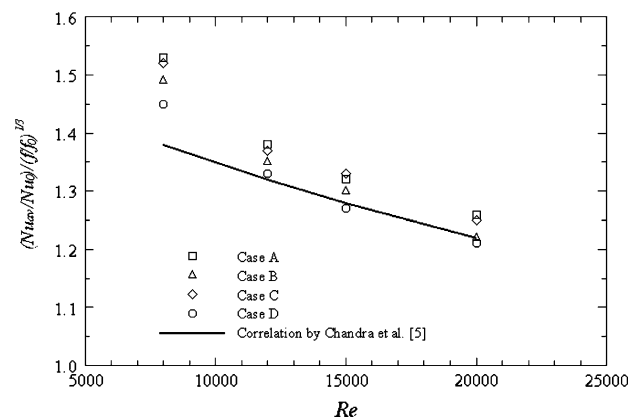


**Fig. 10** Comparison of the thermal performance for various-shaped ribs for  $P/e = 12$

1. For the range of Reynolds number studied, the trapezoidal-shaped ribs with decreasing height in the flow direction (case C) have the highest heat transfer coefficient and friction factor; whereas, the trapezoidal-shaped ribs with increasing height in the flow direction (case D) have the lowest heat transfer performance and pressure drop. In addition, the square-shaped ribs have nearly the same heat transfer and friction characteristics as the triangular-shaped ribs.
2. The local heat transfer is strongly dependent on the rib shape in the region just downstream the rib while this dependence is small in the boundary layer redevelopment zone. The trapezoidal-shaped rib of case C is the most likely one to suppress the local hot spot.
3. The thermal performance is comparable for various-shaped ribs.

**Acknowledgment** The current research is financially supported by the Swedish National Energy Agency (STEM) and Swedish Research Council (VR).

## References

1. Nikuradse J (1950) Law of flow in rough pipes, NACA TM 1292
2. Dipprey DF, Sabersky RH (1963) Heat and momentum transfer in smooth and rough tubes at various Prandtl numbers. *Int J Heat Mass Transf* 6:329–353
3. Webb RL, Eckert ERG, Goldstein RJ (1971) Heat transfer and friction in tubes with repeated-rib roughness. *Int J Heat Mass Transf* 14:601–617
4. Han JC (1984) Heat transfer and friction in channels with two opposite rib-roughened walls. *ASME J Heat Transf* 106:774–781
5. Chandra PR, Alexander CR, Han JC (2003) Heat transfer and friction behaviors in rectangular channels with varying number of ribbed walls. *Int J Heat Mass Transf* 46:481–495
6. Rau G, Cakan M, Moeller D, Arts T (1998) The effect of periodic ribs on the local aerodynamic and heat transfer performance of a straight cooling channel. *ASME J Turbomach* 120:368–375
7. Liou TM, Hwang JJ (1992) Turbulent heat transfer augmentation and friction in periodic fully developed channel flows. *ASME J Heat Transf* 114:56–64
8. Lockett JF, Collins MW (1990) Holographic interferometry applied to rib-roughness heat transfer in turbulent flow. *Int J Heat Mass Transf* 33(11):2439–2449
9. Han JC, Glicksman LR, Rohsenow WM (1978) An investigation of heat transfer and friction for rib-roughened surfaces. *Int J Heat Mass Transf* 21(8):1143–1156
10. Liou TM, Hwang JJ (1993) Effect of ridge shapes on turbulent heat transfer and friction in rectangular channel. *Int J Heat Mass Transf* 36(4):931–940
11. Arman B, Rabas TJ (1992) Disruption shape effect on the performance of enhanced tubes with the separation and reattachment mechanism, ASME Symposium, HTD-202, Enhanced Heat Transfer, 67–75
12. Chandra PR, Fontenot ML, Han JC (1998) Effect of rib profiles on turbulent channel flow heat transfer. *AIAA J Thermophysics Heat Transf* 12(1):116–118
13. Ahn SW (2001) The effect of roughness type on friction factors and heat transfer in roughened rectangular duct. *Int Comm Heat Mass Transf* 28(7):933–942
14. Aliaga DA, Lamb JP, Klein DE (1994) Convection heat transfer distributions over plates with square ribs from infrared thermography measurements. *Int J Heat Mass Transf* 37:363–374
15. Taslim ME, Li T, Kercher DM (1996) Experimental heat transfer and Friction in channels roughened with angled, V-Shaped, and discrete ribs on two opposite walls. *ASME J Turbomachinery* 118:20–28
16. Tanda G (2004) Heat transfer in rectangular channels with transverse and V-shaped broken ribs. *Int J Heat Mass Transf* 47:229–243
17. Wang Z, Ireland PT, Kohler ST, Chew JW (1998) Heat transfer measurements to a gas turbine cooling passage with inclined ribs. *ASME J Turbomachinery* 120:63–69
18. Chang SW, Liou TM, Juan WC (2005) Influence of channel height on heat transfer augmentation in rectangular channels with two opposite rib-roughened walls. *Int J Heat Mass Transf* 48:2806–2813
19. Wang L, Sundén B (2005) Experimental investigation of local heat transfer in a square duct with continuous and truncated ribs. *Exp Heat Transf* 18:179–197
20. Gao X (2002) Heat transfer and fluid flow investigation in ribbed ducts and impinging jets using liquid crystal thermography and PIV, Ph. D. Thesis, Division of Heat Transfer, Lund Institute of Technology, Lund
21. Holman JP (2001) Heat transfer, 9th edn, Chap. 6–2, McGraw-Hill, New York
22. Moffat RJ (1988) Describing the uncertainty in experimental results. *Exp Therm Fluid Sci* 1:3–17
23. Terekhov VI, Yaryina NI, Zhdanov RF (2003) Heat transfer in turbulent separated flows in the presence of high free-stream turbulence. *Int J Heat Mass Transf* 46:4535–4551
24. Papadopoulos G, Ötügen MV (1995) Separating and reattaching flow structure in a suddenly expanding rectangular duct. *ASME J Fluids Eng* 17:17–23